DOI: 10.19884/j.1672-5220.202511006

Water-Soluble NIR-Ⅱ Au∶Ag_2Te Quantum Dots with pH Responsiveness for in vivo Imaging

ZHANG Fenfen[1,2], HE Chuanglong[1*]

1. State Key Laboratory of Advanced Fiber Materials, Shanghai Engineering Research Center of Nano-Biomaterials and Regenerative Medicine, College of Biological Science and Medical Engineering, Donghua University, Shanghai 201620, China
2. Research Center for Analysis and Measurement, Donghua University, Shanghai 201620, China

Abstract: Water-soluble near-infrared-Ⅱ (NIR-Ⅱ) Au-doped Ag_2Te (Au∶Ag_2Te) quantum dots (QDs) with a photoluminescence quantum yield (PLQY) of 9.2% (relative to indocyanine green, ICG) were fabricated via an eco-friendly method. Initially, Ag_2Te QDs were synthesized at ambient temperature by using glutathione as the stabilizer, silver nitrate as the silver source, sodium tellurite as the tellurium source, and sodium borohydride as the reductant. Subsequently, Au∶Ag_2Te QDs were successfully produced by introducing chloroauric acid via a cation exchange mechanism. This approach eliminates the need for organic solvents, high temperatures, and inert gas protection commonly associated with conventional QD synthesis processes. The incorporation of Au effectively mitigates surface defects, enhancing the photoluminescence properties and stability of the hybrid QDs. Additionally, the Au∶Ag_2Te QDs exhibit strong pH responsiveness over the range of pH 5 to 12, with a linear correlation ($R^2 = 0.966\ 5$) between fluorescence intensity and pH. Both in vitro and in vivo evaluations confirmed the distinct fluorescence signals and favorable biocompatibility of the Au∶Ag_2Te QDs, demonstrating their considerable potential for biomedical applications. This research offers a novel strategy for developing water-soluble Au∶Ag_2Te QDs with efficient and stable NIR-Ⅱ fluorescence imaging capability.

Keywords: NIR-Ⅱ quantum dot (QD); Au∶Ag_2Te; pH responsiveness; fluorescence imaging

CLC number: R318.08 **Document code:** A

Article ID: 1672-5220(2026)05-0026-12

0 Introduction

With the rapid advancement of nanomaterials, quantum dots (QDs) have attracted significant attention across various fields, including biomedicine[1-2], optoelectronics[3-4], and energy[5], due to their exceptional optical properties and versatile applications. In particular, near-infrared-Ⅱ (NIR-Ⅱ, 1 000 – 1 700 nm) fluorescence probes have demonstrated remarkable capabilities in bioimaging and disease diagnosis[6-7], owing to their deep tissue penetration and minimal background interference. Among these, Ag_2Te QDs stand out as promising fluorescence probes because of their superior NIR-Ⅱ emission properties[8-10]. For example, Chen et al.[11] developed a thiolate etching technique using 1-dodecanethiol as a ligand to facilitate the interaction between silver(Ⅰ) and tellurium in cubic-phase PbTe QDs, leading to their decomposition and the formation of homogeneous Ag_2Te. The synthesized Ag_2Te QDs exhibited fluorescence emission at 1 300 nm, low toxicity, and a photoluminescence quantum yield (PLQY) of 7%. However, this method required high temperatures and organic solvents, rendering the process complex. To enhance the fluorescence imaging capabilities of Ag_2Te QDs, researchers have employed various strategies, including cation exchange, surface modification, core/shell structure construction, and ligand engineering to fabricate Zn-, Bi-, and Mn-doped Ag_2Te QDs[12-14]. Yang et al.[15] reported the synthesis of Au-doped Ag_2Te (Au∶Ag_2Te) QDs via a cation exchange method, achieving NIR-Ⅱb fluorescence emission at 1 600 nm and a 12-fold increase in fluorescence intensity compared to pure Ag_2Te QDs. However, this synthesis involved toxic reagents such as tributyl phosphite, 1-(3-dimethylaminopropyl)-3-ethylcarbodiimide hydrochloride, and chloroform, along with complex procedures. Additionally, Zhou et al.[16] employed silver ions to mitigate surface defects, resulting in water-soluble Ag_2Te QDs with a six-fold enhancement in fluorescence intensity; nevertheless, the PLQY of the resulting material was only 8.0%. In light of these findings, conventional methods for synthesizing Au∶Ag_2Te QDs often rely on organic solvents, high-temperature reactions, and inert gas protection, which not only complicate the preparation process but also raise environmental concerns. Moreover, issues such as

Received date: 2025-11-20

Foundation items: National Natural Science Foundation of China (Nos. 32271412 and 32071350)

* Correspondence should be addressed to HE Chuanglong, email: hcl@dhu.edu.cn

Citation: Zhang F F, He C L. Water-soluble NIR-Ⅱ Au∶Ag_2Te quantum dots with pH responsiveness for in vivo imaging[J]. *Journal of Donghua University (English Edition)*, 2026, 43(5): 26-37.

surface defects and limited stability hinder their practical applications. Consequently, the development of environmentally friendly, simple, and efficient strategies for QD fabrication has become a central focus of contemporary research[17-18].

Water-soluble QDs have gradually emerged as a research hotspot due to their facile synthesis and eco-friendliness. This study aims to develop a novel method for synthesizing water-soluble Au∶Ag_2Te QDs by incorporating green chemistry principles. Glutathione (GSH) is used as the stabilizer. Silver nitrate and sodium tellurite serve as the silver and tellurium sources, respectively, and sodium borohydride acts as the reductant. Under mild conditions, Ag_2Te QDs are successfully prepared. Additionally, a cation exchange strategy is employed to introduce chloroauric acid, resulting in the synthesis of Au∶Ag_2Te QDs. Experimental results demonstrate that Au incorporation effectively reduces surface defects, significantly enhancing the fluorescence performance and stability of the hybrid QDs. Moreover, Au∶Ag_2Te QDs exhibit excellent pH-responsive properties, showing a strong linear relationship ($R^2 = 0.966\ 5$) between fluorescence intensity and pH values in the range of 5 to 12. Both in vitro and in vivo studies confirm the superior fluorescence signals and biocompatibility of Au∶Ag_2Te QDs. In summary, this study not only introduces a novel, environmentally sustainable approach to the synthesis of Au∶Ag_2Te QDs but also paves a way for developing highly efficient and stable NIR-Ⅱ fluorescence probes, offering new insights for versatile material applications.

1 Materials and Methods

1.1 Materials

Chloroauric acid ($HAuCl_4$) and sodium tellurite (Na_2TeO_3) were obtained from Shanghai Meryer Biochemical Technology Co., Ltd., China. GSH was purchased from Adamas-Beta Company, China. Silver nitrate ($AgNO_3$), sodium borohydride ($NaBH_4$), sodium hydroxide (NaOH), hydrochloric acid (HCl), and other routine chemicals were supplied by Sinopharm Chemical Reagent Co., Ltd., China. The calcein-AM/PI cell viability/cytotoxicity assay kit and cell counting Kit-8 (CCK-8) were supplied by Beyotime Biotechnology, China. Fetal bovine serum (FBS), RPMI-1640, and penicillin-streptomycin were acquired from Thermo Fisher Scientific, USA.

1.2 Synthesis of QDs

1.2.1 Synthesis of Ag_2Te QDs

The synthesis of Ag_2Te QDs began with the sequential addition of 0.32 mmol of $AgNO_3$, 0.38 mmol of GSH, and 1.50 mmol of NaOH into a conical flask containing 50 mL of deionized water at 25 ℃. Under continuous stirring at 1 300 r/min, a clear and transparent solution formed. Subsequently, 0.16 mmol of Na_2TeO_3 was introduced into the solution, followed by an additional 30 min of stirring to ensure complete homogenization. Then, 6.5 mg of $NaBH_4$ was added to the reaction system. Serving as the reductant, $NaBH_4$ efficiently converted tellurite ions (TeO_3^{2-}) into telluride ions (Te^{2-}), which then combined with silver ions (Ag^+) to form Ag_2Te QDs. Upon continuous agitation for another 2 h, the mixture gradually evolved into a homogeneous yellowish-brown solution, indicating the formation of Ag_2Te QDs.

1.2.2 Fabrication and purification of Au∶Ag_2Te QDs

To the as-synthesized Ag_2Te QDs, 0.32 mmol of $HAuCl_4$ was introduced, followed by the addition of NaOH to adjust pH to 11. Stirring was maintained for 60 min until brown-colored Au∶Ag_2Te QDs were obtained. The QDs were subsequently dialyzed using a dialysis bag with a molecular weight cutoff (MWCO) of 1 000 g/mol at 25 ℃ for at least 24 h for purification. Finally, the purified products were stored at 4 ℃ for subsequent applications.

1.3 Characterization of Au∶Ag_2Te QDs

Transmission electron microscopy (TEM) and high-resolution TEM (HRTEM) images were acquired using a JEM-2100F instrument (JEOL, Japan) operated at 200 kV. Ultraviolet-visible-near infrared (UV-Vis-NIR) spectra, dynamic light scattering (DLS) profiles, and fluorescence spectra were measured using a UV-3600 spectrophotometer (Shimadzu, Japan), a BI-200SM instrument (Brookhaven, USA), and a steady-state/transient fluorescence spectrometer (QM/TM, PTI, USA), respectively, after appropriately diluting the QDs. The fluorescence images were captured by the NIR-Ⅱ imaging system at an excitation wavelength of 808 nm with a power density of 100 mW/cm^2. Fourier transform infrared (FTIR) spectra, X-ray diffraction (XRD) patterns, and X-ray photoelectron spectroscopy (XPS) were obtained from freeze-dried samples by using an iS50 FTIR spectrometer (Thermo Fisher Scientific, USA), a D8 XRD diffractometer (Bruker, Germany), and an Escalab 250Xi XPS system (Thermo Fisher Scientific, USA), respectively. The contents of Au, Ag, and Te were quantified by inductively coupled plasma optical emission spectroscopy (ICP-OES) using a Prodigy Plus instrument (Leeman, USA).

1.4 In vitro biocompatibility assessment

Human umbilical vein endothelial cells (HUVECs) were obtained from the Cell Bank of the Chinese Academy of Sciences and seeded into 24-well culture plates at a density of 5×10^4 cells per well. The cells were cultured in complete RPMI-1640 medium supplemented with 10% (volume fraction) FBS and 1% (volume fraction) penicillin/streptomycin, and then incubated at 37 ℃ with 5% (volume fraction) CO_2 for 24 h. After cell attachment, Au∶Ag_2Te QDs were added to achieve final mass concentrations of 0 (control), 10, 25, and 50 μg/mL, with three replicates per group. The cells were then cultured for an additional three days. Subsequently, an appropriate volume of calcein-AM/PI double-staining

solution was added. Following incubation at 37 ℃ for 15–20 min in the dark, cell viability and death were observed using a fluorescence microscope. Thereafter, a specific volume of CCK-8 reagent was added to each well. After 30 min of incubation, the absorbance at 450 nm was measured to quantitatively assess cell proliferation.

1.5 In vivo imaging efficacy and safety assessment in mice

Animal experiments were conducted in accordance with established ethical standards and approved by the Animal Ethics Committee of Donghua University (No. DHUEC-NSFC-2022-27). Eight-week-old male Institute of Cancer Research (ICR) mice were anesthetized via intraperitoneal injection of 10% (mass fraction) chloral hydrate. The experimental group received 200 μL of Au∶Ag_2Te QDs at a mass concentration of 200 μg/mL via the tail vein, while the control group received no treatment. Imaging was performed using an NIR-Ⅱ imaging system (NIR-Ⅱ-ST, Shanghai Digi-united Biotechnology Co., Ltd., China) with an 808 nm laser at a power density of 200 mW/cm^2 and an exposure time of 200 ms.

To evaluate the acute toxicity of Au∶Ag_2Te QDs, changes in the body mass of mice were monitored at 24, 48, and 72 h post-injection. Simultaneously, key organs, including the heart, liver, spleen, lung, and kidney, were harvested on day 3 and subjected to hematoxylin-eosin (H&E) staining to detect whether there were abnormal morphological alterations in the tissues.

1.6 Statistical analysis

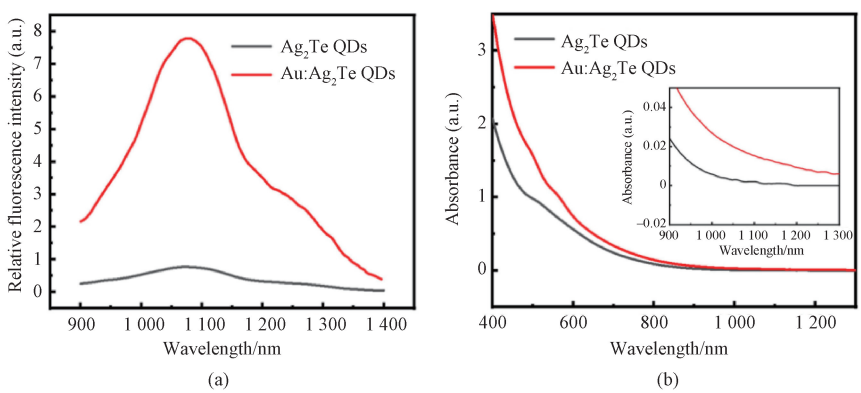
All data were statistically analyzed by using Origin Pro 2018 and expressed in the format of mean ± standard deviation with three replicates per group (n=3). One-way analysis of variance (ANOVA) and Tukey's method were employed to assess overall differences among groups. Statistical significance was set at p<0.001.

2 Results and Discussion

2.1 Structural characteristics of Au∶Ag_2Te QDs

In this study, a novel method was employed to synthesize water-soluble Au∶Ag_2Te QDs at 25 ℃, using GSH as the stabilizer, $AgNO_3$ as the silver source, Na_2TeO_3 as the tellurium source, and $NaBH_4$ as the reductant. Subsequently, a cation doping strategy was implemented by introducing chloroauric acid, which effectively reduced surface defects and significantly enhanced the photoluminescence intensity and stability of the Au∶Ag_2Te QDs. Various characterization techniques, including TEM, DLS, FTIR, fluorescence, UV-Vis-NIR, XRD, XPS, and ICP-OES, were employed to comprehensively investigate the morphological and structural properties of the synthesized QDs.

As shown in the fluorescence emission spectra (Fig. 1(a)), Au incorporation enhances the photoluminescence intensity of Au∶Ag_2Te QDs by approximately eightfold compared to Ag_2Te QDs, accompanied by a 7 nm hypsochromic shift in the emission wavelength (from 1 077 nm to 1 070 nm). The UV-Vis-NIR absorption spectra (Fig. 1(b)) confirm higher absorption values for Au∶Ag_2Te QDs than pristine Ag_2Te QDs across the 400–1 300 nm range. Figure 1(c) shows the visual photographs of these QDs. As presented, Ag_2Te QDs exhibit a yellowish-brown appearance with relatively low fluorescence imaging signal strength. Conversely, Au∶Ag_2Te QDs display a deep brown color. The NIR-Ⅱ imaging system is subsequently employed to assess the fluorescence imaging performance of Au∶Ag_2Te QDs. Imaging results are presented in Fig. 1(d). The fluorescence imaging signal of Au∶Ag_2Te QDs is significantly enhanced compared to Ag_2Te QDs. This finding further confirms that Au incorporation exerts a prominent enhancing effect on the fluorescence intensity of Au∶Ag_2Te QDs. Additionally, the PLQY of Au∶Ag_2Te QDs is determined to be 9.2% relative to indocyanine green (ICG) in dimethyl sulfoxide (DMSO), exceeding the previously reported values of 6.2%[15] and 3.2%[19], thereby facilitating their applications.



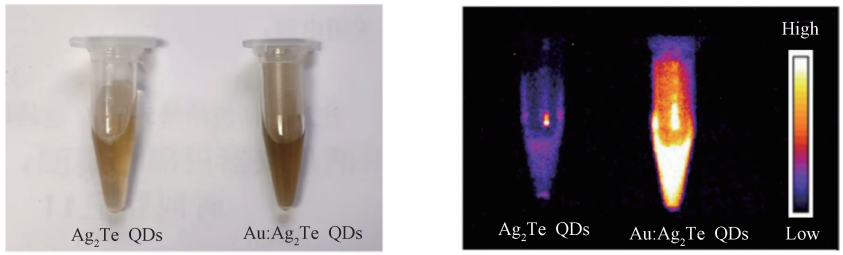


Fig. 1 Spectroscopic characterizations of Ag_2Te and Au∶Ag_2Te QDs: (a) fluorescence emission spectra; (b) UV-Vis-NIR absorption spectra; (c) photographs of QDs in water; (d) fluorescence images

The TEM image (Fig. 2(a)) reveals that Au∶Ag_2Te QDs exhibit a spherical morphology with a monodisperse and uniform distribution. HRTEM (Fig. 2(b)) demonstrates the lattice spacing of Au∶Ag_2Te QDs is 0.21 nm, aligning well with the $(\bar{2}21)$ plane of monoclinic Ag_2Te[16], confirming the crystalline structure of Au∶Ag_2Te QDs. The average particle size of Au∶Ag_2Te QDs is determined to be (2.75 ± 0.03) nm (Fig. 2(c)). Furthermore, the DLS result (Fig. 2(d)) indicates a hydrodynamic diameter of (4.12 ± 0.74) nm, suggesting the presence of a hydration layer on the surface of the hybrid Au∶Ag_2Te QDs.

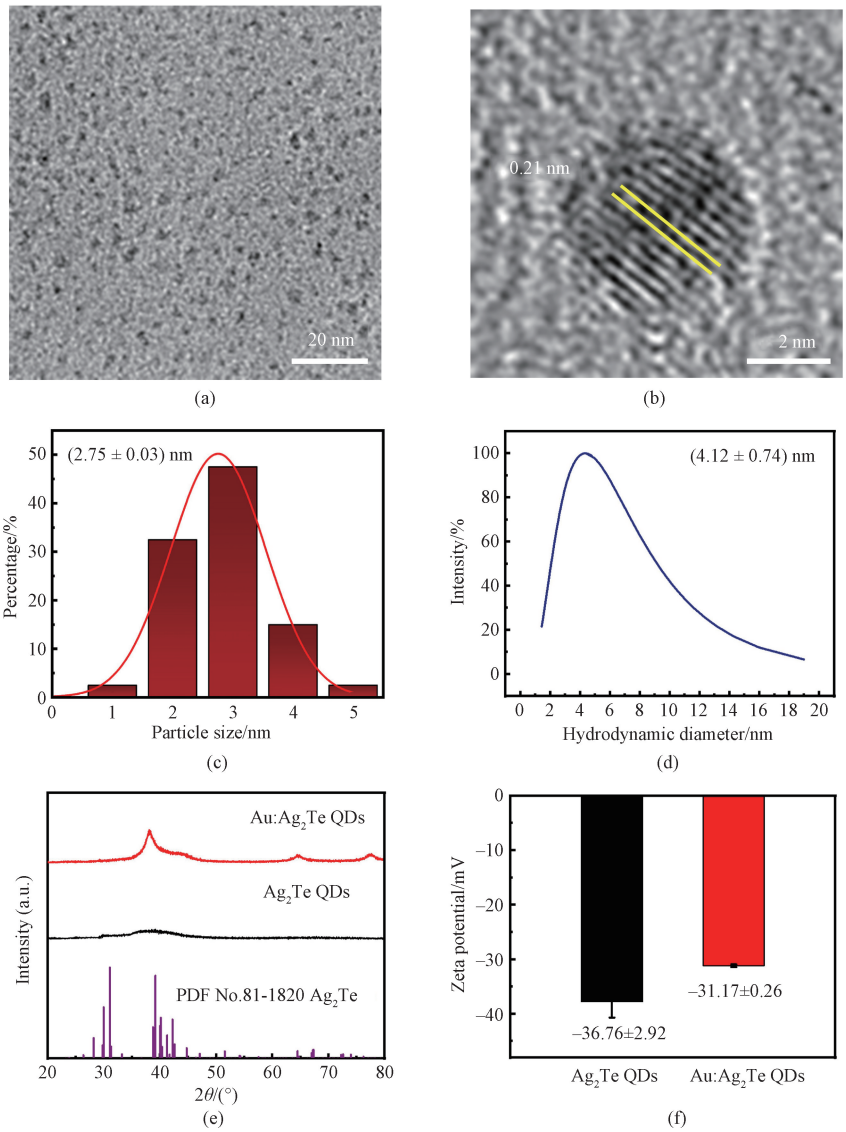


Fig. 2 Characterizations of Au∶Ag_2Te QDs: (a) TEM image; (b) HRTEM image; (c) particle size distribution obtained from TEM image analysis; (d) hydrodynamic diameter distribution measured by DLS; (e) XRD patterns; (f) zeta potential

The XRD patterns are depicted in Fig. 2(e). Although the diffraction peak signals are relatively weak, the diffraction profile of Au∶Ag_2Te QDs is consistent with that of monoclinic-phase Ag_2Te, indicating that the incorporation of Au does not alter the crystal structure of Ag_2Te QDs[15]. The dispersion stability of QDs in aqueous solutions can be evaluated via zeta potential, where a higher absolute zeta potential value reflects enhanced colloidal stability of the QDs. The zeta potentials of Ag_2Te and Au∶Ag_2Te QDs are (−36.76 ± 2.92) mV and (−31.17 ± 0.26) mV (Fig. 2(f)), respectively, confirming their good stability in aqueous environments. Moreover, the slight positive deviation in the zeta potential of Au∶Ag_2Te QDs proves the successful incorporation of the Au element.

The XPS spectra confirm the presence of Au in Au∶Ag_2Te QDs, which is absent in Ag_2Te QDs (Fig. 3(a)), thereby verifying the successful synthesis of Au∶Ag_2Te QDs. High-resolution spectra further identify the presence of Au 4f, Ag 3d, Te 3d, S 2p, and C 1s orbitals in Au∶Ag_2Te QDs (Figs. 3(b)–(f)). Specifically, peaks at 87.8 eV and 84.2 eV correspond to the Au $4f_{5/2}$ and Au $4f_{7/2}$ orbitals[20], indicating both Au(0) and Au(I) are present[15], in alignment with the zeta potential data. Peaks at 374.0 eV and 368.0 eV are assigned to Ag $3d_{3/2}$ and Ag $3d_{5/2}$ orbitals, confirming the +1 oxidation state of Ag. Similarly, peaks at 586.6 eV and 576.2 eV are attributed to Te $3d_{3/2}$ and Te $3d_{5/2}$ orbitals, suggesting a −2 oxidation state of Te[13]. The S 2p orbital peaks at 162.3 eV and 162.7 eV indicate coordination of sulfur in GSH with Ag^+ and Au^+, while the orbital peak at 164.0 eV corresponds to free thiol groups[21-22]. Additionally, the C 1s binding energy is split into peaks at 287.9 eV and 284.8 eV, representing carbonyl and methylene carbons, respectively, indicating exposed carboxyl groups that contribute to water solubility.

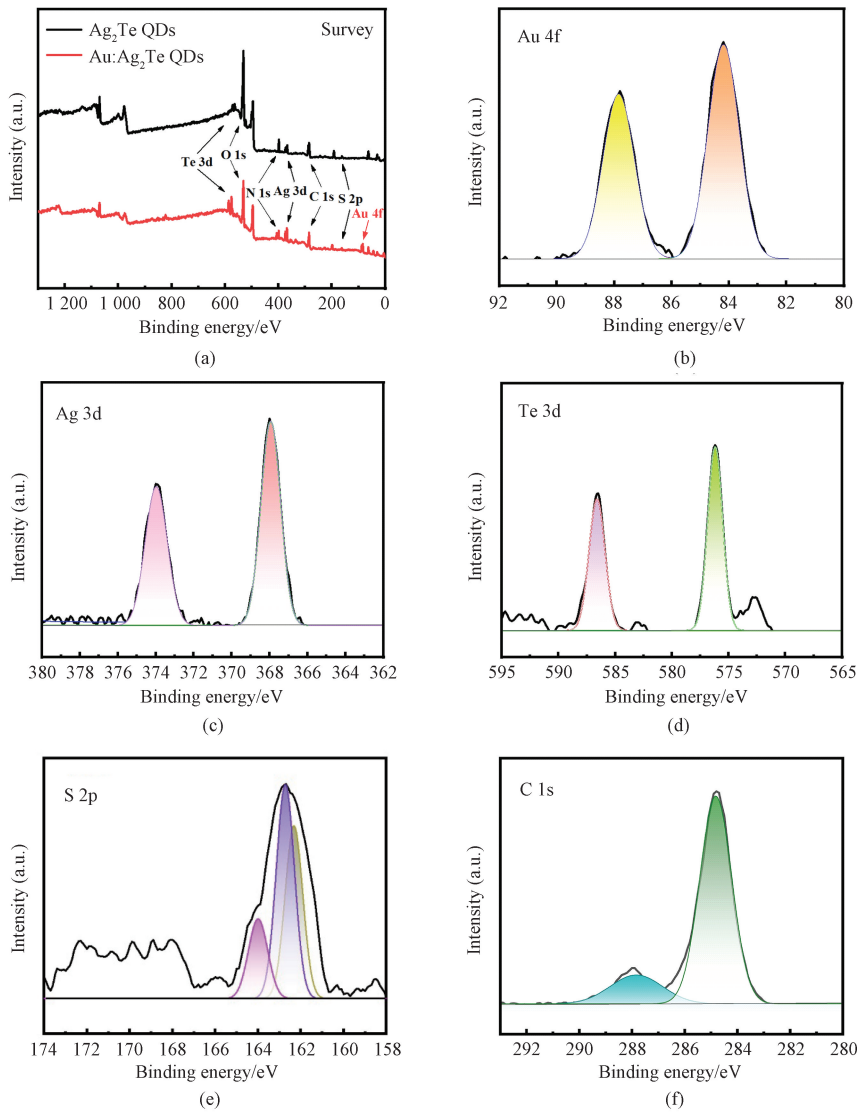


Fig. 3 Valence states of QDs detected by XPS: (a) XPS spectra of Ag_2Te and Au∶Ag_2Te QDs; high-resolution XPS spectra of (b) Au 4f, (c) Ag 3d, (d) Te 3d, (e) S 2p, and (f) C 1s in Au∶Ag_2Te QDs

ICP-OES analysis was conducted to quantify the elemental composition of Ag_2Te and Au∶Ag_2Te QDs (Table 1). For Ag_2Te QDs, the molar ratio of Ag to Te was determined to be 2.23∶1.00; for Au∶Ag_2Te QDs, the molar ratio of Au to Ag to Te was 0.98∶2.06∶1.00. These results demonstrate that the Au doping level increases significantly during the cation exchange reaction, with the cation-to-anion ratio exceeding the stoichiometric ratio of 2∶1. This phenomenon is presumably associated with the ultra-small size and ultra-large specific surface areas of Au∶Ag_2Te QDs, which collectively promote the stable binding of Au and Ag ions on their surfaces to thiol groups.

Table 1 Quantitative content of Au, Ag, and Te elements determined by ICP-OES

Sample	Mass concentration/(μg/mL)			Molar ratio of Au∶Ag∶Te
	Au	Ag	Te	
Ag_2Te	0	18.98	10.06	0∶2.23∶1
Au∶Ag_2Te	17.31	19.94	11.47	0.98∶2.06∶1

FTIR spectra were employed to elucidate the stabilizing effect of GSH on Au∶Ag_2Te QDs (Fig. 4). The spectrum of Au∶Ag_2Te QDs exhibits characteristic absorption peaks similar to those of GSH: the peak at 2 932 cm^{-1} corresponds to the stretching vibration of —CH_2; the absorption bands observed at 1 601 cm^{-1} and 1 384 cm^{-1} correspond to the asymmetric and symmetric stretching of —COOH, respectively; and the peak at 1 121 cm^{-1} represents the stretching vibration of C—N[23]. Notably, the S—H peak at 2 523 cm^{-1}, a signature of GSH, disappears in Au∶Ag_2Te QDs, indicating the formation of stable coordination bonds between sulfur atoms and Ag or Au[24]. Additionally, the double peaks of the amide I band at 3 256 cm^{-1} and 3 349 cm^{-1} in GSH merge into a broad peak within the range of 3 300–3 500 cm^{-1} in Au∶Ag_2Te QDs, suggesting potential coordination interactions between nitrogen atoms and Au or Ag[25]. In conclusion, the FTIR results demonstrate that GSH plays a crucial role in stabilizing the Au∶Ag_2Te nanostructure. Beyond the primary coordination of the thiol group, the amino, amide, and carboxyl groups in GSH may also contribute to stabilizing Au∶Ag_2Te QDs through coordination interactions. Specifically, the electronegative nature of the carboxyl group enables effective interaction with positively charged Ag or Au, thereby enhancing the stability of Au∶Ag_2Te QDs.

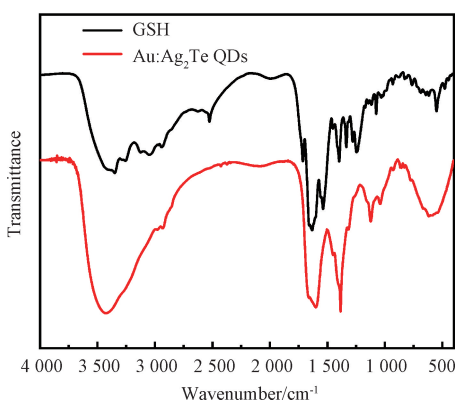


Fig. 4 FTIR spectra of GSH and Au∶Ag_2Te QDs

2.2 Tunable photophysical properties of Ag_2Te and Au∶Ag_2Te QDs

The optimal performance of QDs is highly dependent on ligand content. In this study, water-soluble Ag_2Te QDs were synthesized in an alkaline environment by using GSH as the stabilizer. $AgNO_3$ and Na_2TeO_3 were fixed at 0.32 mmol and 0.16 mmol, respectively, while the GSH addition was varied by adjusting the molar ratios of GSH to $AgNO_3$ to 0.9∶1, 1.2∶1, and 1.5∶1. This approach aimed to investigate how different GSH amounts affect the fluorescence emission spectra of Ag_2Te QDs. As shown in Fig. 5(a), increasing the GSH-to-$AgNO_3$ molar ratio from 0.9∶1 to 1.2∶1 results in a gradual increase in the relative fluorescence intensity of Ag_2Te QDs, with the maximum emission peak shifting slightly from 1 077 nm to 1 074 nm. However, further increasing the molar ratio to 1.5∶1 causes a decrease in fluorescence intensity and a blue shift of the emission peak to 1 071 nm. This behavior is attributed to optimal coordination between GSH and Ag at the 1.2∶1 molar ratio. In contrast, excess GSH at a higher molar ratio leads to ligand competition for cationic coordination, reducing fluorescence intensity and inducing a blue shift in the emission peak. Based on these results, the GSH-to-$AgNO_3$ molar ratio is set at 1.2∶1.

Previous studies have demonstrated that cationic doping effectively modulates the photophysical properties of QDs[12,26]. To address the low fluorescence intensity of pristine Ag_2Te QDs, a systematic Au doping strategy is employed by adding $HAuCl_4$ (0.16, 0.32, and 0.48 mmol) to the optimized synthesis system ($AgNO_3$: 0.32 mmol; Na_2TeO_3: 0.16 mmol; GSH: 0.38 mmol). As shown in Fig. 5(b), the greatest fluorescence enhancement occurs at an Au-to-Ag molar ratio of 1∶1 ($HAuCl_4$: 0.32 mmol), accompanied by a 4 nm blue shift in the emission peak, which shifts from 1 074 nm to 1 070 nm. The actual Au-to-Ag molar ratio, determined by ICP-OES, is about 0.48∶1 (Table 1). Excessive Au doping (0.48 mmol) results in fluorescence quenching, with relative fluorescence intensity returning to levels observed in undoped samples. In summary, moderate Au

incorporation mitigates surface defects in the hybrid QDs, whereas excessive doping causes competitive coordination between Au and Ag ions for GSH, leading to lattice distortion and subsequent fluorescence quenching.

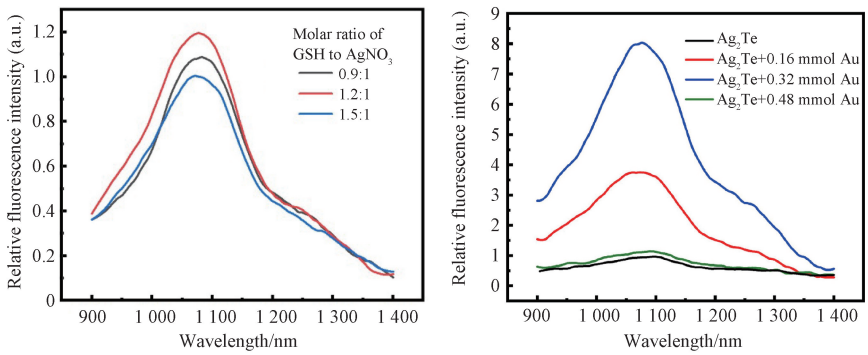


Fig. 5 Fluorescence performance: (a) effect of molar ratios (0.9∶1, 1.2∶1, 1.5∶1) of GSH to $AgNO_3$ on fluorescence properties of Ag_2Te QDs; (b) effect of Au contents (0.16, 0.32, and 0.48 mmol) on fluorescence properties of Au∶Ag_2Te QDs

2.3 Photostability of Au∶Ag_2Te QDs

In addition to the colloidal dispersion stability in the solution, the photostability of QDs is also crucial for their practical applications. Therefore, the photostability of Au∶Ag_2Te QDs was investigated. Specifically, indocyanine green (ICG) was dissolved in DMSO, and both ICG and Au∶Ag_2Te QDs were irradiated with an 808 nm laser at 100 mW/cm^2 for varying durations. As shown in Fig. 6, after 120 min of irradiation, the fluorescence intensity of ICG decreases significantly to (40.21 ± 0.35)% of its initial value, whereas Au∶Ag_2Te QDs retain (94.33 ± 0.16)% of their original signal. This marked difference demonstrates the superior photostability of Au∶Ag_2Te QDs, providing a solid experimental foundation for their use in biomedical imaging and photothermal therapy.

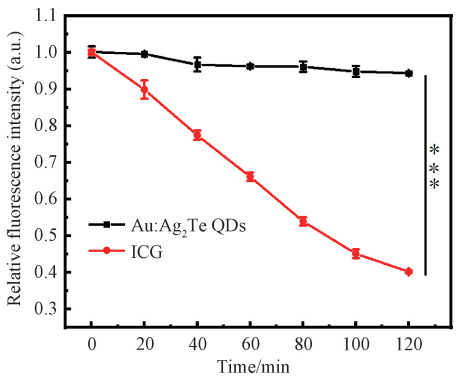


Fig. 6 Photostability of Au∶Ag_2Te QDs and ICG (*** represents $p < 0.001$)

2.4 pH responsiveness of Au∶Ag_2Te QDs

In biomedical research, pH monitoring is crucial for drug development, disease diagnosis, treatment monitoring, and cell culture[27-28]. Therefore, we investigated the correlation between the fluorescence properties of Au∶Ag_2Te QDs and pH. Notably, the fluorescence intensity of Au∶Ag_2Te QDs varies significantly with pH, indicating a pH-dependent modulation mechanism of their optical properties. Au∶Ag_2Te QDs were initially synthesized at a pH of 8, after which the pH was adjusted to 1–7 using HCl and to 9–12 using NaOH, respectively. We observed that Au∶Ag_2Te QDs were unstable when pH was 1–4, precipitating after 24 h, while remaining stable when pH was 5–12. Consequently, our analysis focused on the fluorescence intensity of Au∶Ag_2Te QDs at pH 5–12.

As shown in Fig. 7, the fluorescence intensity of Au∶Ag_2Te QDs peaks when pH is 5. With increasing pH, the fluorescence intensity gradually decreases, exhibiting a linear correlation with pH ($R^2 = 0.9665$). A slight red shift of the maximum emission peak is also observed. This behavior is attributed to structural changes in GSH under varying pH conditions, which alter the binding interactions between GSH and the QDs. This also constitutes the rationale for our selection of GSH as the stabilizer in QD synthesis.

Specifically, under strongly acidic conditions (pH≤4), the carboxyl groups of GSH fail to undergo deprotonation, remaining in their neutral —COOH configuration, while the amino groups are protonated to form positively charged $—NH_3^+$ groups[29]. As a consequence, the GSH acquires a weak positive charge in the highly acidic media, so it triggers intense homo-charge repulsion between GSH and the Ag^+/Au^+ cations of QDs, which in turn breaks the coordination interaction, resulting in ligand desorption from the surface of QDs. The removal of ligand coating significantly compromises both the steric stabilization and charge screening capacities of the QDs, eliminating the critical safeguard that maintains the colloidal dispersion of Au∶Ag_2Te QDs. With repulsive forces diminished, van der Waals attractions and electrostatic interactions take over as the primary interparticle forces[30-31]. This causes the originally monodispersed QDs to collide frequently and aggregate into large agglomerates, eventually leading to precipitation (Fig. 8(a)).

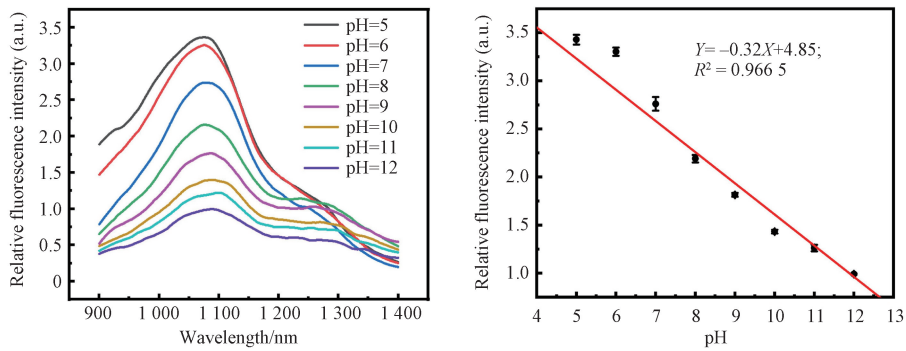


Fig. 7 pH responsiveness of Au:Ag_2Te QDs: (a) fluorescence spectra at pH of 5–12; (b) fitted curve of relative fluorescence intensity (Y) vs. pH (X)

As presented in Fig. 8(b), at pH = 5, GSH's carboxyl groups are fully deprotonated to —COO^-, amino groups remain as protonated —NH_3^+, and thiol groups are electrically neutral, rendering GSH nearly neutral overall with a compact, rigid conformation[32]. This structure allows GSH to form stable coordination bonds with QDs' Ag^+/Au^+ via thiols, while —COO^- enables auxiliary anchoring electrostatically, building a dense "dual-site anchored" ligand layer. The layer fully covers surface dangling bonds and lattice defects to minimize non-radiative recombination centers, and its compact conformation avoids steric hindrance to carrier radiative transitions, resulting in the QDs' maximum fluorescence intensity[33-34]. As pH rises, the —NH_3^+ group of GSH is gradually deprotonated to —NH_2, and the thiol group converts to negatively charged —S^-, changing GSH from zwitterion to anion with a conformation switch from compact to extended (Figs. 8(c)–8(d)), which is consistent with the results in Ref. [35]. Though —S^- enhances GSH-metal coordination, the extended conformation creates ligand layer gaps, exposing surface defects and slightly increasing non-radiative recombination. The enhanced GSH negativity induces QDs' surface charge redistribution, and the local electric field interferes with electron-hole pair recombination, reducing radiative efficiency. Additionally, partial —S^- competes with —OH^- for surface sites, causing ligand desorption and more defects, ultimately leading to a decrease in fluorescence intensity.

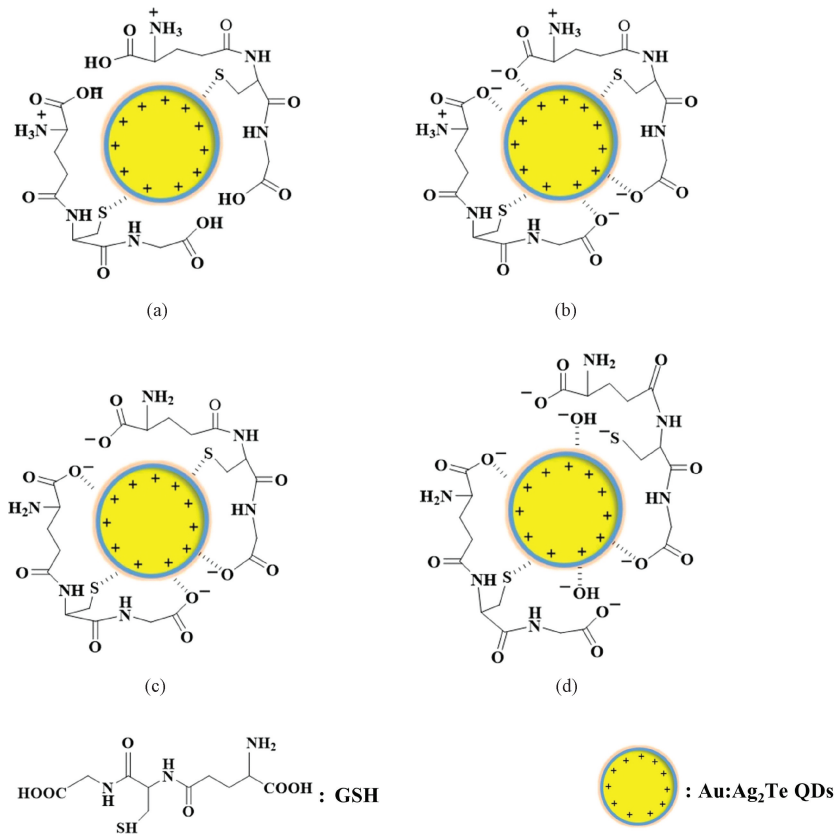


Fig. 8 Interaction mechanism between GSH and Au:Ag_2Te QDs under varying pH conditions: (a) pH ≤ 4; (b) pH = 5; (c) pH = 6–7; (d) pH ≥ 8

2.5 In vitro biocompatibility of Au∶Ag_2Te QDs

The biocompatibility of materials is a crucial prerequisite for in vivo applications[36-37]. Therefore, the biocompatibility of Au∶Ag_2Te QDs was evaluated using HUVECs. Results shown in Fig. 9(a) reveal that all HUVECs maintain cellular activity when the mass concentrations of Au∶Ag_2Te QDs range from 0 to 50 μg/mL, with calcein-AM/PI staining indicating no significant cell death. The CCK-8 assays (Fig. 9(b)) demonstrate a similar trend, showing comparable proliferative capacity across all groups. Zhou et al.[12] indicated that the viability of HT22 cells and bEnd.3 cells would be impaired when the mass concentration of Zn∶Ag_2Te QDs exceeded 50 μg/mL. Our findings reveal that Au∶Ag_2Te QDs do not inhibit HUVECs proliferation within the mass concentration range of 0 to 50 μg/mL, demonstrating that the prepared Au∶Ag_2Te QDs possess favorable biocompatibility.

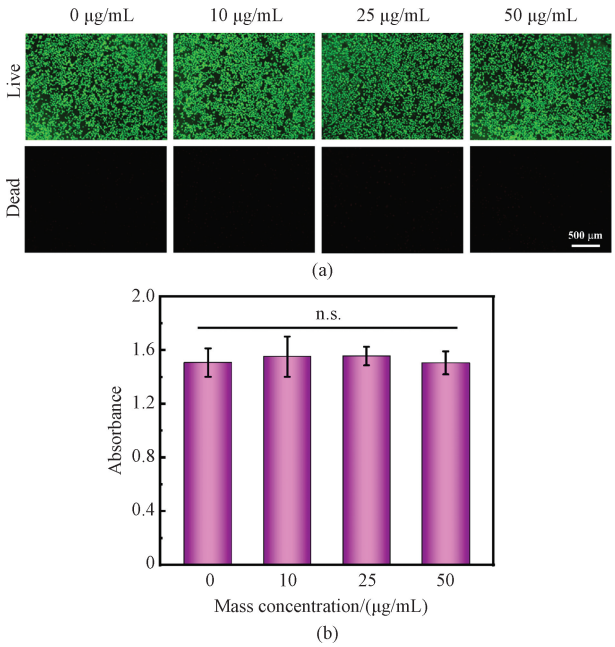


Fig. 9 Biocompatibility assessment of Au∶Ag_2Te QDs using HUVECs: (a) live/dead cell staining; (b) proliferation of HUVECs detected by CCK-8 (n. s. denotes not significant)

2.6 Imaging efficacy of Au∶Ag_2Te QDs in vivo

Leveraging the superior fluorescence imaging, stability, and biocompatibility of Au∶Ag_2Te QDs, their in vivo imaging potential was investigated. No imaging signals are detected in control mice without Au∶Ag_2Te QDs (Fig. 10(a)). In contrast, there are distinct fluorescence signals in the liver and bladder regions of mice in both prone (Fig. 10(b)) and supine (Fig. 10(c)) positions within 2 h following injection of Au∶Ag_2Te QDs. These results demonstrate the excellent tissue penetration and imaging capabilities of Au∶Ag_2Te QDs, supporting their potential application in non-invasive tissue detection.

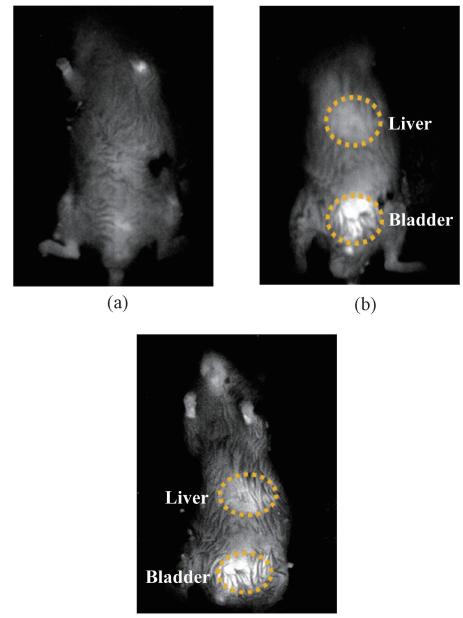


Fig. 10 In vivo imaging ability of Au∶Ag_2Te QDs: (a) control group; (b) experimental group in prone position; (c) experimental group in supine position

2.7 Acute toxicity evaluation of Au∶Ag_2Te QDs

Ag_2Te QDs have demonstrated significant advantages in chemistry, bioimaging, disease monitoring, and related fields. However, literature on their in vivo safety remains limited[38]. This study conducted a systematic assessment of the biosafety of the synthesized Au∶Ag_2Te QDs following tail vein administration in mice. As shown in Fig. 11(a), both treated and control groups exhibit consistent body mass gain throughout the observation period, with no significant differences. H&E staining further reveals no observable pathological changes in major organs, including the heart, liver, spleen, lung, and kidney of Au∶Ag_2Te QDs-treated mice compared to the control group (Fig. 11(b)). These results indicate that the synthesized Au∶Ag_2Te QDs exhibit excellent biosafety at the tested dose, which further validates the dispersion stability of these nanomaterials (Fig. 2(f)). Specifically, no aggregation occurs to form large-sized clusters, thereby preventing the induction of localized oxidative stress; moreover, no acute toxic responses are observed, thus laying a solid safety foundation for their subsequent biomedical applications.

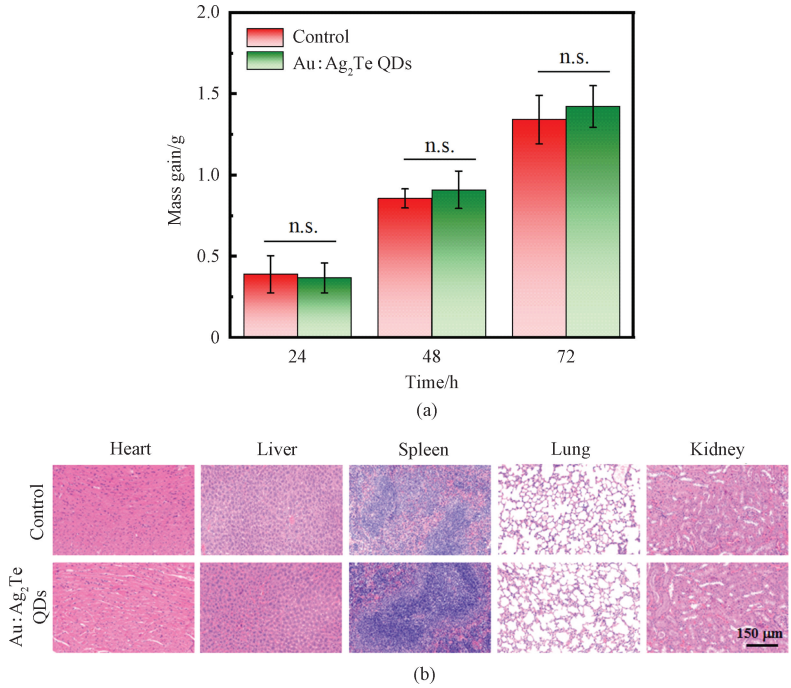


Fig. 11 Acute toxicity evaluation of Au∶Ag_2Te QDs: (a) mass changes of mice at 24, 48, and 72 h after tail vein injection of Au∶Ag_2Te QDs; (b) H&E staining of major organs collected at 72 h

3 Conclusions

This research successfully developed water-soluble NIR-Ⅱ Au∶Ag_2Te QDs through a simple and efficient synthesis process. The optimized synthesis system ($AgNO_3$: 0.32 mmol; Na_2TeO_3: 0.16 mmol; GSH: 0.38 mmol) combined with moderate Au doping (Au/Ag molar ratio of 1∶1) effectively addressed the weak fluorescence intensity of pristine Ag_2Te QDs, resulting in hybrid QDs with high fluorescence intensity, excellent yield, and remarkable stability. Moreover, Au∶Ag_2Te QDs exhibited superior pH responsiveness across a broad pH range of 5 to 12. This pH-dependent optical behavior is attributed to the protonation and deprotonation of GSH's carboxyl and amino groups under varying pH conditions, which modulates the interaction between GSH and QDs and influences the stability of the latter. Both in vitro and in vivo experiments confirm the excellent biosafety of these multifunctional QDs. Overall, the stable, pH-responsive, and biocompatible NIR-Ⅱ Au∶Ag_2Te QDs developed in this study offer a promising platform for applications in biomedical imaging, pH monitoring, and related therapeutic fields.

References

[1] Meng X S, Song J W, Meng H W, et al. Microenvironment-activatable nanoagent for real-time NIR-Ⅱ monitoring and targeted therapy of arterial restenosis [J]. *Biomaterials*, 2026, 324: 123482.

[2] Bandaru S, George N, Sharma B, et al. Aqueous based ultra-small magnetic Cr-doped CdSe quantum dots as a potential dual imaging probe in biomedicine [J]. *Biomaterials Science*, 2024, 12(24): 6338-6350.

[3] Kiani M S, Parkhomenko H P, Mangrulkar M, et al. Stepping toward portable optoelectronics with SnO_2 quantum dot-based electron transport layers [J]. *ACS Omega*, 2023, 8(23): 21212-21222.

[4] Houtepen A J, Sargent E H, Infante I, et al. Colloidal quantum dots for optoelectronics [J]. *Nature Reviews Methods Primers*, 2025, 5(1): 42.

[5] Suganya G, Arivanandhan M, Kalpana G. A facile synthesis of PbS-G QDs nanocomposite as electrode material with enhanced energy density for high performance supercapattery application [J]. *Journal of Inorganic and Organometallic Polymers and Materials*, 2022, 32(6): 2135-2145.

[6] Geng H C, Wang C H, Dong Y T, et al. In vivo dynamic monitoring and photothermal therapy of bacterial infection by NIR-Ⅱ $CuInSe_2$ quantum dots [J]. *Chemical Engineering Journal*, 2025, 508: 160924.

[7] Zhang P, Wang Y R, Liu X T, et al. Carboxyl-modified quantum dots for NIR-Ⅱb bone marrow imaging [J]. *ACS Applied Materials & Interfaces*, 2024, 16(7): 8509-8517.

[8] Li B J, Wang G H, Tong Y J, et al. Noninvasive gastrointestinal tract imaging using BSA-Ag_2Te quantum dots as a CT/NIR-Ⅱ fluorescence dual-modal imaging probe in vivo [J]. *ACS Biomaterials Science & Engineering*, 2023, 9(1): 449-457.

[9] Zhang Z Y, Yang H C, Wang M Z, et al. NIR-Ⅱ silver-based quantum dots: synthesis and applications [J]. *Nano Research*, 2024, 17(12): 10620-10643.

[10] Shi X H, Dai Y Y, Wang L, et al. Water-soluble high-quality Ag_2Te quantum dots prepared by mutual adaptation of synthesis and surface modification for in vivo imaging [J]. *ACS Applied Bio Materials*, 2021, 4(10): 7692-7700.

[11] Chen S, Tang T, Huang B, et al. Thiolate etching route for the ripening of uniform Ag_2Te quantum dots emitting in the second near-infrared window: implication for noninvasive in vivo imaging [J]. *ACS Applied Nano Materials*, 2022, 5(3): 3415-3421.

[12] Zhou Y F, Huang B, Chen S H, et al. Ultra-bright near-infrared-Ⅱb emitting Zn-doped Ag_2Te quantum dots for noninvasive monitoring of traumatic brain injury [J]. *Nano Research*, 2023, 16(2): 2719-2727.

[13] Dai P, Wang Z X, Tang Z Y, et al. Bismuth-doped Ag_2Te colloidal quantum dots for high-performance shortwave-infrared photodetectors [J]. *Inorganic Chemistry*, 2025, 64(28): 14637-14643.

[14] Huang B, Tang T, Chen S H, et al. Near-infrared-Ⅱb emitting single-atom catalyst for imaging-guided therapy of blood-brain barrier breakdown after traumatic brain injury [J]. *Nature Communications*, 2023, 14: 197.

[15] Yang H C, Huang H Y, Ma X, et al. Au-doped Ag_2Te quantum dots with bright NIR-Ⅱb fluorescence for in situ monitoring of angiogenesis and arteriogenesis in a hindlimb ischemic model [J]. *Advanced Materials*, 2021, 33(37): 2103953.

[16] Zhou J Q, Huang Y, Zhang Z L, et al. Water-soluble Ag_2Te quantum dots with emission in the second near-infrared window [J]. *Chemical Journal of Chinese Universities*, 2021, 42(6): 2072-2079. (in Chinese)

[17] Cui M J, Huang Q M, Huang W Y, et al. Preparation of water-soluble Sm∶ZnO-NH_2 QDs fluorescent probe and its application for selective detection of dopamine [J]. *Chinese Journal of Luminescence*, 2023, 44(2): 374-386. (in Chinese)

[18] Wu J, Li J H, Li L, et al. Water-soluble near-infrared $CuInS_2$/ZnS fluorescent quantum dots for Cu^{2+} detection and cellular imaging [J]. *Microchemical Journal*, 2024, 199: 109962.

[19] Zheng W S, Gao G B, Deng H, et al. Room temperature synthesis and near-infrared fluorescence performance optimization of Ag_2Se@Ag_2S core-shell quantum dots [J]. *Acta Chimica Sinica*, 2023, 81(7): 763-770. (in Chinese)

[20] Ou X L, Wang Z, Yu D J, et al. VEGF-loaded ROS-responsive nanodots improve the structure and function of sciatic nerve lesions in type Ⅱ diabetic peripheral neuropathy [J]. *Biomaterials*, 2025, 315: 122906.

[21] Peng B, Zheng L X, Wang P Y, et al. Physical origin of dual-emission of Au-Ag bimetallic nanoclusters[J]. *Frontiers in Chemistry*, 2021, 9: 756993.

[22] Castner D G, Hinds K, Grainger D W. X-ray photoelectron spectroscopy sulfur 2p study of organic thiol and disulfide binding interactions with gold surfaces [J]. *Langmuir*, 1996, 12(21): 5083-5086.

[23] Yu Y L, Xu L R, Chen J, et al. Hydrothermal synthesis of GSH-TGA co-capped CdTe quantum dots and their application in labeling colorectal cancer cells [J]. *Colloids and Surfaces B: Biointerfaces*, 2012, 95: 247-253.

[24] Balavandy S K, Shameli K, Biak D R B A, et al. Stirring time effect of silver nanoparticles prepared in glutathione mediated by green method [J]. *Chemistry Central Journal*, 2014, 8: 11.

[25] Yang J, Zhang W H, Hu Y P, et al. Aqueous synthesis and characterization of glutathione-stabilized β-HgS nanocrystals with near-infrared photoluminescence [J]. *Journal of Colloid and Interface Science*, 2012, 379(1): 8-13.

[26] Moslem S S, El-Komy G M, El-Khawas E H, et al. Effect of Fe doping on structural, optical and magnetic properties of CdS quantum dots [J]. *Physica Scripta*, 2025, 100(3): 035916.

[27] Dong W C, Xue X, Yang H K, et al. Construction of a cellulose-based dual-responsive fluorescent probe for simultaneous pH and HClO detection and imaging in arthritic mice [J]. *Sensors and Actuators B: Chemical*, 2026, 448(2): 138940.

[28] Sonawane P M, Jain N, Roychaudhury A, et al. In-vivo monitoring of macrophage mitochondrial pH dynamics in zebrafish using an ultrasensitive and water-soluble targeted fluorescent sensor [J]. *Talanta*, 2026, 298: 128963.

[29] Vallée A, Humblot V, Méthivier C, et al. Glutathione adsorption from UHV to the liquid phase at various pH on gold and subsequent modification of protein interaction [J]. *Surface and Interface Analysis*, 2008, 40(3/4): 395-399.

[30] Rani N, Singh P, Kumar S, et al. Plant-mediated synthesis of nanoparticles and their

applications: a review [J]. *Materials Research Bulletin*, 2023, 163: 112233.
[31] Lv X F, Shi T R, Bai X, et al. A simple and efficient colorimetric detection of creatinine based on citrate-stabilized gold nanoparticles [J]. *Plasmonics*, 2025, 20(5): 2753-2763.
[32] Chen W B, Guéguen C, Smith D S. Assessing effects of pH, metal ion and natural organic matter on identification and determination of reduced glutathione by cathodic stripping voltammetry [J]. *International Journal of Environmental Analytical Chemistry*, 2017, 97(4): 330-344.
[33] Wu H F, Wang Q Q, Dong M C, et al. pH-responsive dual-emission carbon dots for the ratiometric detection of organophosphorus pesticides in Brassica chinensis and Hg^{2+} in water [J]. *Food Chemistry*, 2024, 454: 139755.
[34] Kim H J, Shin M H, Hong H G, et al. Enhancement of optical efficiency in white OLED display using the patterned photoresist film dispersed with quantum dot nanocrystals [J]. *Journal of Display Technology*, 2016, 12(6): 526-531.
[35] Jia K, Jin Y H, Liu S Q, et al. The application and mechanism of degradable activator biologically small molecule organic acids in smithsonite flotation [J]. *Applied Surface Science*, 2024, 660: 159907.
[36] Wang Z, Yu F, Jiang Y X, et al. Comparative study on chitosan modified with different hepatocyte ligands as scaffold material for liver tissue regeneration: preparation, characterization and evaluation [J]. *Journal of Donghua University* (*English Edition*), 2024, 41(3): 263-274.
[37] Gao Z, Liu Y, Wang C, et al. Hippocampal neuron-derived extracellular matrix coated nanofibrous scaffold for neural tissue engineering [J]. *Journal of Donghua University* (*English Edition*), 2019, 36(5): 431-436.
[38] Zhang J Z, Tang H, Chen X Z, et al. In vivo fate of Ag_2Te quantum dot and comparison with other NIR-Ⅱ silver chalcogenide quantum dots [J]. *Journal of Nanoparticle Research*, 2020, 22(9): 287.

pH 响应的水溶性 NIR-Ⅱ区 Au∶Ag_2Te 量子点用于生物体内成像

张芬芬[1,2], 何创龙[1*]

1. 东华大学 先进纤维材料全国重点实验室, 上海纳米生物材料与再生医学工程技术研究中心, 生物与医学工程学院, 上海 201620

2. 东华大学 分析测试中心, 上海 201620

摘　要: 通过一种环保的方法制备了水溶性近红外-Ⅱ区(near-infrared-Ⅱ, NIR-Ⅱ)量子点, Au 掺杂 Ag_2Te (Au∶Ag_2Te)。以吲哚菁绿(indocyanine green, ICG)为对照, 其光致发光量子产率(photoluminescence quantum yield, PLQY)达到 9.2%。先以谷胱甘肽为稳定剂、硝酸银为银源、亚碲酸钠为碲源、硼氢化钠为还原剂在室温下制备了 Ag_2Te 量子点。随后, 通过阳离子交换机制引入氯金酸, 成功合成了 Au∶Ag_2Te 量子点。该方法避免了传统量子点合成过程中所需的有机溶剂、高温和惰性气体保护。金元素的引入有效抑制了表面缺陷, 提高了 Au∶Ag_2Te 量子点的光致发光性能和稳定性。此外, 在 pH 为 5 ~ 12 时, Au∶Ag_2Te 量子点表现出强烈的 pH 响应性, 荧光强度与 pH 值之间存在线性相关性(R^2 = 0.966 5)。体内外研究证实了该复合量子点具有明显的荧光信号和良好的生物相容性, 在生物医学应用中具有较大潜力。该研究为开发具有高效、稳定的 NIR-Ⅱ荧光成像能力的水溶性 Au∶Ag_2Te 量子点提供了新策略。

关键词: 近红外-Ⅱ区量子点; Au∶Ag_2Te; pH 响应; 荧光成像